Journal of Power Sources 196 (2011) 10207–10212

Contents lists available at SciVerse ScienceDirect

Journal of Power Sources

journal homepage: www.elsevier.com/locate/jpowsour

Enhancing Ni–Sn nanowire lithium-ion anode performance by tailoring active/inactive material interfaces

Miao Tian [1], Wei Wang [1], Se-Hee Lee [1], Yung-Cheng Lee [1], Ronggui Yang [*,1]

Department of Mechanical Engineering, University of Colorado, Boulder, CO 80309, USA

ARTICLE INFO

Article history:
Received 11 June 2011
Received in revised form 12 August 2011
Accepted 13 August 2011
Available online 22 August 2011

Keywords:
Lithium-ion battery
Anode material
Tin-based intermetallics
Nanowire arrays

ABSTRACT

Nanowire arrays have attracted great attention due to their great potential to improve the performance of Li-ion batteries. In this work, we studied anode performance of lithium-ion batteries using Ni–Sn nanowire arrays. A versatile method through a porous anodic alumina (PAA) template-assisted electrochemical deposition process was developed to directly synthesize Ni–Sn nanowire arrays on copper current collectors. This method presents significant advantage that the as-prepared Ni–Sn nanowire arrays can be directly used as anode electrode without any binder or conductive materials. However, the formation of a continuous Ni–Sn film at the base of the nanowires result in quick loss of electrical contact between the active material and the current collector because of the large strain mismatch at the large continuous active/inactive material (A/I) interface. By growing short Cu nanoscrews as a buffer layer before Ni–Sn nanowire growth, the formation of Ni–Sn film was inhibited and the A/I interface was scaled down to nanoscale islands. The strain mismatch is thus significantly reduced, which results in enhanced structural stability and battery performance. The effect of the composition and the length of Ni–Sn nanowire arrays on the electrochemical performance of lithium ion batteries are also systematically studied.

1. Introduction

Nanostructured electrodes have great potential in significantly improving the performance of rechargeable Li-ion batteries which have been widely used as power sources for cell phones [1], laptop computers [2], and electric vehicles [3–7]. Among various nanostructures, nanowire electrodes have recently attracted great interests [8–10]. Many features of nanowires lead to significant improvements in battery performance: (1) the free spaces between nanowires provide easy access of the electrolyte to all the surfaces of the electrode and accommodate volume changes during lithium ion insertion; (2) the small diameter of nanowires allows for fast Li-ion diffusion and high power delivery; (3) direct connection of nanowires to the current collector ensures direct transportation of electrons to the current collector, which eliminates the necessity of any binder materials or conducting additives [11,12]. Electrodes with nanowires of various materials such as Si, TiO_2, Fe_3O_4, SnO_2, Co_3O_4, and V_2O_5 [11,13–17] have been studied and show improved performance compared to bulk electrodes.

The interface between the active material and the inactive current collector has also been found important for electrodes. It has been shown that failure of Si film anode is due to delaminating of Si film from the Cu substrate, isolating the electronic pathways from Si to the underlying Cu [18]. Similar phenomenon was observed for Sn alloy films [19]. Annealing and modification of current collector surfaces could improve the adhesion between the active material and the current collector and thus make the reversible capacity high and stable [20–22]. On the other hand, battery stability can also be improved by scaling down the heterogeneous interface of Si and carbon nanotubes [23]. The critical role of the active/inactive material interfaces (A/I interfaces) in electrodes can be systematically studied using nanowires since their unique structure offers a way to tailor the A/I interfaces.

In this study, we used a facile method with the assistance of free-standing porous anodic alumina (PAA) templates to fabricate high-aspect ratio Ni–Sn nanowire arrays directly on current collectors. PAA template, produced by electrochemical oxidation of aluminum, is widely used to fabricate nanowire arrays due to the tunability and the compatibility with various materials [24,25]. Ni–Sn nanowire arrays with different A/I interface areas were realized to study the effect of A/I interface scaling on the electrochemical performance. The effect of the composition and the

* Corresponding author. Tel.: +1 303 735 1003; fax: +1 303 492 3498.
E-mail addresses: mmtian@colorado.edu (M. Tian), wei.wang-1@colorado.edu (W. Wang), Sehee.Lee@colorado.edu (S.-H. Lee), leeyc@colorado.edu (Y.-C. Lee), ronggui.yang@colorado.edu (R. Yang).
[1] DARPA Center for Integrated Micro/Nano-Electromechanical Transducers (iMINT), USA.

0378-7753/$ – see front matter © 2011 Elsevier B.V. All rights reserved.
doi:10.1016/j.jpowsour.2011.08.062

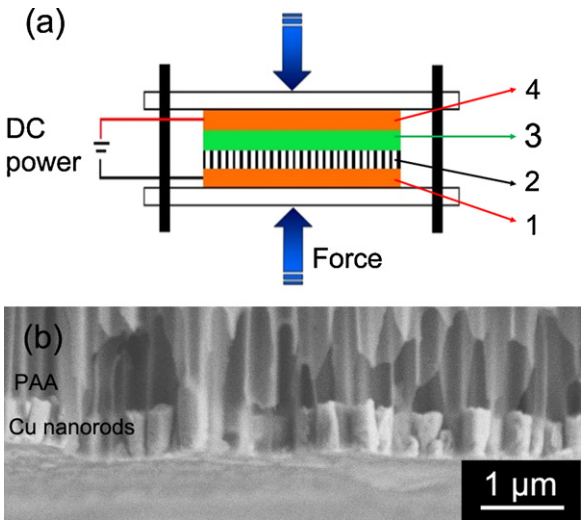

Fig. 1. (a) Schematics of the sandwich structure used for electroplating short nanorods to bond the PAA template on the Cu substrate: 1 – copper foil which serves as current collector and as the substrate of nanowire arrays, 2 – PAA template, 3 – filter paper saturated with electrolyte solution, and 4 – copper plate which serves as counter electrode. (b) Short Cu nanorods deposited in the PAA template which bonds PAA template on Cu substrate for the second electroplating step.

length of Ni–Sn nanowires on the electrode performance were also systematically studied.

2. Experimental

Commercial and homemade PAA templates were used for the synthesis of Ni–Sn nanowire arrays. The commercial PAA templates (Anodisc 47, Whatman 6809-5522) have an average pore diameter of 200 nm. The homemade PAA templates with an average pore diameter of 80 nm were obtained by anodizing high-purity (5 N) aluminum foil at 40 V in 0.3 M oxalic acid for 24 h at 5 °C.

A two-step electrochemical deposition process was developed to directly grow nanowire arrays on Cu current collector.

The first step is to electrochemically deposit short nanorods to bond the PAA template onto the Cu substrate. Fig. 1 shows a typical sandwich-structure setup for this step. A constant voltage was applied between the Cu substrate and the counter-electrode for a certain time to grow short nanorods, which serve as "nanoscrews" to bond the PAA template onto the Cu substrate for the second step three-electrode electrochemical deposition. Two kinds of materials, intermetallic Ni–Sn or Cu, were electroplated as the bonding materials for different Ni–Sn nanowire on Cu current collector samples. For Ni–Sn bonding, the deposition was conducted at voltage of −1 V for 10 min and the electrolyte consisted of 17.82 g L^{-1} $NiCl_2{\cdot}6H_2O$, 39.4 g L^{-1} $SnCl_2{\cdot}2H_2O$, 165.15 g L^{-1} $K_4P_2O_7$, and 9.38 g L^{-1} glycine, with an addition of NH_4OH 5 mL L^{-1} for pH value control [26]. For Cu bonding, the deposition was conducted at voltage of −0.8 V for 10 min and the electrolyte consisted of 6 g L^{-1} cupric pyrophosphate ($Cu_2P_2O_7{\cdot}xH_2O$; Sigma–Aldrich 344699), 25 g L^{-1} potassium pyrophosphate ($K_4P_2O_7$, Sigma–Aldrich 322431), and 2 g L^{-1} ammonium citrate ($C_6H_{17}N_3O_7$, Fluka 09831) [27]. Fig. 1b shows the short Cu nanoscrews grown in this step with length of ~0.6 μm. Similar nanorods of Ni–Sn with a length of ~1 μm were observed when intermetallic Ni–Sn is deposited as the bonding material.

In the second step, Ni–Sn nanowires were fabricated by co-depositing Sn and Ni in a three-electrode glass cell filled with the same Ni–Sn electrolyte as that in the first step. An Ag/AgCl electrode immersed in the saturated KCl solution was used as a reference electrode, and a Pt coil was used as the counter-electrode for three-electrode electrochemical deposition. The potentiostatic deposition was performed on a CHI 760c electrochemical work station. After electrochemical deposition, the final Ni–Sn nanowire array samples were obtained after immersing in 1 M NaOH solution to dissolve the PAA templates and cleaning with DI water.

The field emission scanning electron microscope (FE-SEM, JEOL's JSM-7401F) with energy-dispersive X-ray spectroscopy (EDS) option was employed to study the morphology and composition of the nanowires. X-ray diffraction spectrometer (Scintag PAD5) with Cu Kα radiation (1.54056 Å) was used to record the XRD patterns. The as-prepared Ni–Sn nanowire arrays on Cu current collector were tested in the electrolyte containing 1 M $LiPF_6$ in ethylene carbonate (EC)/dimethyl carbonate (DMC) (1:1 volume ratio, Aldrich), with Li foil (Alfa Aesar) as counter-electrode. The CR2032 coin-type cells were assembled in an argon-filled glove box system (Vacuum Atmosphere Nexus model) and tested with a computer controlled potentiostats/galvanostats system (Arbin BT-2000). The discharge–charge experiments were performed galvanostatically within the voltage window of 0.02–1.5 V (vs. Li/Li+).

3. Results and discussion

Fig. 2 shows the difference between the Ni–Sn nanowire arrays with two kinds of PAA template bonding materials. When Ni–Sn nanorods were used for bonding in the first step (Fig. 2(a)), a thin film of intermetallic Ni–Sn was formed in the gap between the PAA template and the Cu substrate due to the roughness on copper surface, which resulted in a large continuous A/I interface. The FE-SEM image of Ni–Sn nanowires on Cu current collector confirms the formation of continuous Ni–Sn film. In the other structure, Cu nanoscrews were used to bond the PAA template onto Cu substrate (Fig. 2(b)). Cu film was formed in the gap between the PAA template and the Cu substrate, followed by Cu nanoscrews in nanopores of the PAA (Fig. 1(b)), which reduces the A/I interface (Ni–Sn/Cu interface) to nanoscale islands on top of Cu nanoscrews. The FE-SEM image in Fig. 2(b) shows that the A/I interface is confined to the cross-section of each nanowire.

Fig. 3(a) and (b) shows the FE-SEM images of Ni–Sn nanowire arrays with a characteristic nanowire diameter of ~200 nm and ~80 nm, respectively. The length of the nanowires is controlled by adjusting the electrochemical deposition time, and the diameter is determined by the pore size of PAA templates, as shown in the inset figures. The nanowires are agglomerated, and micro-scale gaps are formed between nanowire clusters due to the high aspect ratio. In the XRD spectrum of the as-prepared Ni–Sn nanowires in Fig. 3(c), peaks of Ni_3Sn_4 alloy can be clearly identified, indicating that Ni_3Sn_4 is the predominant phase in the intermetallic Ni–Sn, consistent with reported results of electrodeposited Ni–Sn [28,29]. The peak of Cu comes from the Cu current collector. The EDS spectrum in Fig. 3(d) shows that the as-prepared Ni–Sn nanowire arrays contain about 82 wt% Sn.

Fig. 4(a) shows the discharge capacity over cycle number for Ni–Sn nanowire array anodes with different bonding materials at the base. The capacities of the electrodes using both Ni–Sn nanowire arrays drop substantially after the first cycle. Similar observation has been reported for most Sn based materials [30], due to the formation of solid-electrolyte interphase (SEI) and the irreversible decomposition of intermetallic Ni–Sn during the activation step. Much higher capacity is observed for Ni–Sn nanowire arrays with Cu nanoscrews at the base than that of Ni–Sn nanowire arrays with Ni–Sn film bonding, especially after the second cycle. FE-SEM image (Fig. 4(b)) shows that the Ni–Sn nanowires with Cu nanoscrews at the base maintain intact on the Cu current collector after 30 cycles. However, a large number of nanowires fell off from the Cu

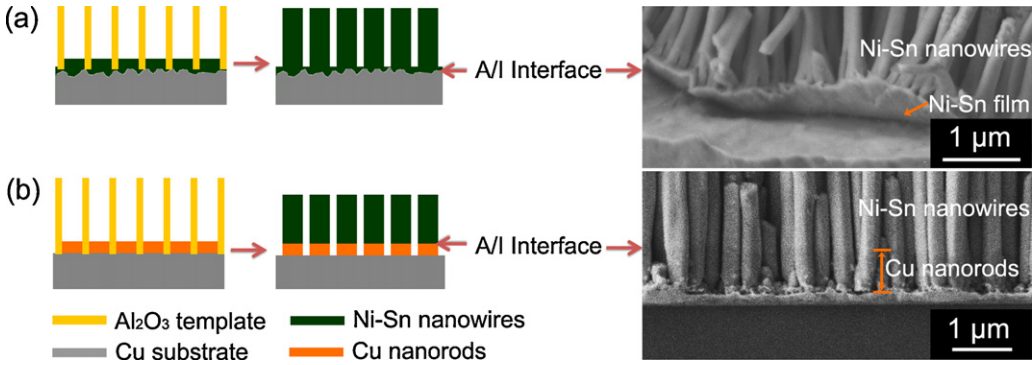

Fig. 2. Schematics and FE-SEM images of Ni–Sn nanowire arrays with different bonding materials at base: (a) Ni–Sn bonding and (b) Cu bonding.

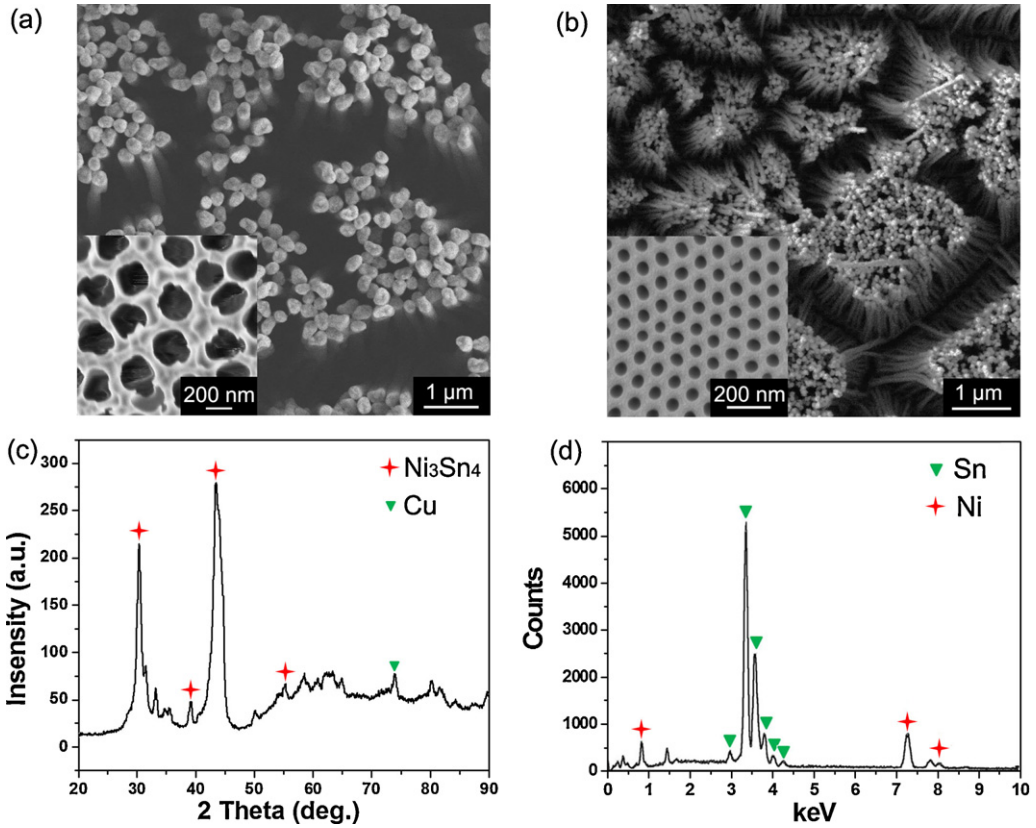

Fig. 3. (a) Ni–Sn nanowire arrays with a nanowire diameter of ~200 nm using a commercial PAA template (inset: PAA template with 200 nm pore diameter). (b) Ni–Sn nanowire arrays with a nanowire diameter of ~80 nm using a home-made PAA template (inset: PAA template with 80 nm pore diameter). (c) X-ray diffraction (XRD) spectrum of ~200 nm Ni–Sn nanowire arrays. (d) energy-dispersive X-ray spectroscopy (EDS) spectrum of ~200 nm Ni–Sn nanowire arrays.

current collector after 10 cycles for the sample with Ni–Sn bonding film at the base, as shown in Fig. 4(c), although all the nanowires are still intact. Since the only difference between the two samples is the materials at the base of Ni–Sn nanowires, the comparison clearly shows that the Ni–Sn film at the base resulted in the failure of Ni–Sn nanowires electrode. The reason for the failure could be due to the large strain mismatch resulted from the large A/I interface introduced by the continuous Ni–Sn film [31,32]. However, in the Ni–Sn nanowire arrays with Cu bonding, the A/I interface area is reduced to nanoscale island as shown in Fig. 2, which significantly reduces the strain mismatch and thus improves the electrochemical performance of the Ni–Sn nanowire electrodes. The capacity was improved and the Ni–Sn nanowires were retained on Cu current collector after 30 cycles. We can preliminary conclude from the above comparison that electrode performance can be improved by scaling down A/I interface area.

To confirm the above observations and to further improve the battery performance, we further reduced the interface area between the active Ni–Sn nanowires and inactive Cu current collector by adjusting the nanowire diameters of the Cu nanoscrew-bonded Ni–Sn nanowire samples. When the diameter of nanowires decreases, the A/I interface area which is the same as cross-sectional area of the nanowires also decreases. Fig. 5(a) shows discharge capacities of electrodes using different diameter Ni–Sn nanowire arrays with Cu nanoscrew bonding. During the first 30 cycles, similar capacity was measured for nanowires with 200 nm and 80 nm diameters. However, the specific capacity of 200 nm-diameter nanowires drops dramatically after 30 cycles while that of 80 nm-diameter nanowires mostly retains. This indicates that Ni–Sn nanowires with smaller diameter have better cycle stability. One possible reason for the better cycle stability observed could be that smaller nanowires can accommodate better the volume

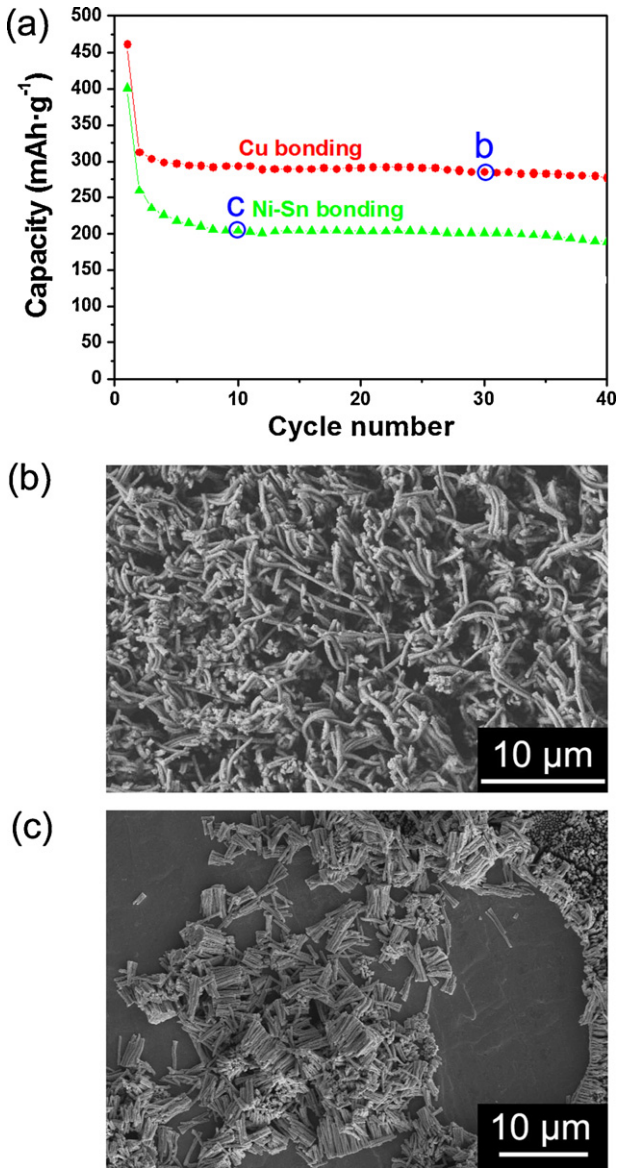

Fig. 4. (a) Electrochemical performance of Li-ion batteries using Ni–Sn nanowires with Cu bonding and with Ni–Sn bonding as anodes. The nanowire diameter in both samples is around 200 nm, and the length is around 8 μm. Material load for both samples is 1.55 mg cm^{-2}. Test current is 50 mA g^{-1}. (b) FE-SEM image of the Cu bonded Ni–Sn nanowires after 30 cycles. (c) FE-SEM image of the Ni–Sn film bonded Ni–Sn nanowires after 10 cycles.

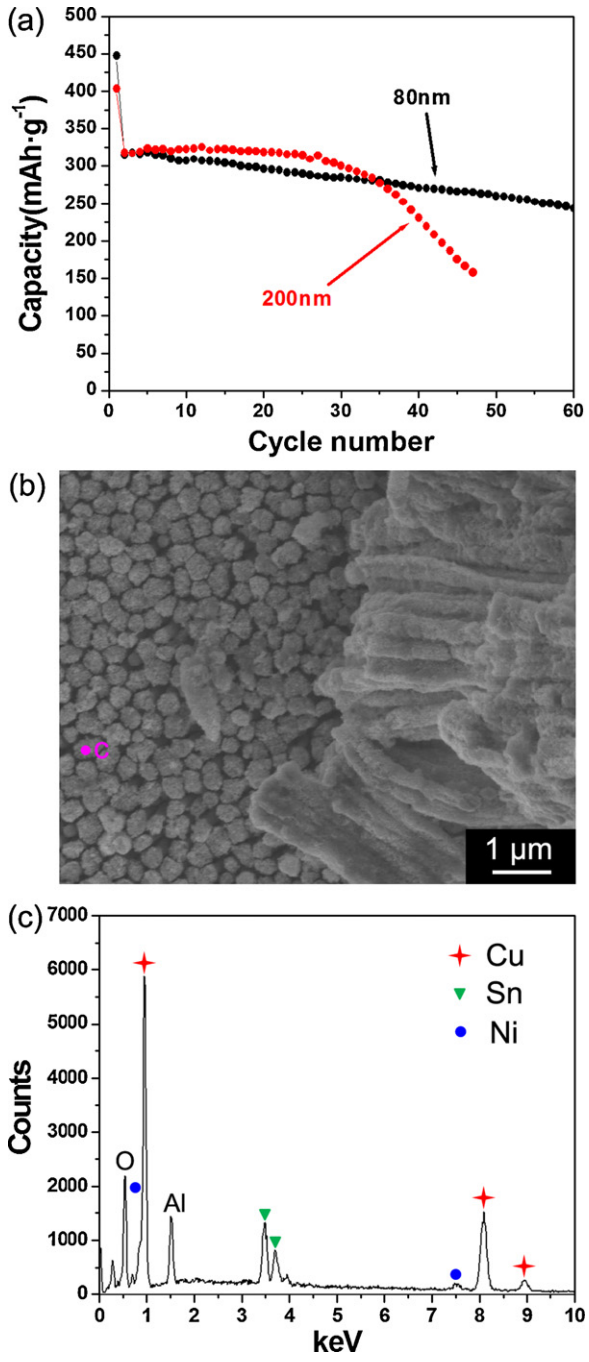

Fig. 5. (a) Discharge capacity of Cu nanorod-bonded Ni–Sn nanowire arrays with different diameters. Test current is 50 mA g^{-1} and Ni–Sn nanowire length is ~8 μm. (b) FE-SEM image of the electrode with 200 nm-diameter Cu nanorods-bonded Ni–Sn nanowire arrays after 48 cycles of test. (c) EDS spectrum from the position c in (b).

change during lithium insertion and release processes because of the reduced diffusion-induced stress, as reported in theoretical studies [33]. However, this is not the main reason here. Fig. 5(b) shows the FE-SEM image of the 200 nm-diameter Ni–Sn nanowire electrode after 48 discharge–charge cycles. Ni–Sn nanowires (bundles on right side) lost contact from the current collector, leaving short Cu nanoscrews (on left side) on the substrate. EDS spectrum taken from the position c in Fig. 5(b) confirms that the nanostructures remaining on the substrates are Cu nanoscrews, as shown in Fig. 5(c). From the above results, the well-retained nanowire structures confirm that pulverization from diffusion-induced stress is not the failure mechanism for the 200 nm-diameter Ni–Sn nanowires. Furthermore, comparing with Fig. 4(b), the drop of the capacity for the 200 nm-diameter nanowire sample after 35 cycles is due to the fall-off of Ni–Sn nanowires from the Cu current collector, which resulted from an unstable A/I interface. Ni–Sn nanowires swell and shrink during the charge-discharge process, causing the strain mismatch at the A/I interface since the inactive current collector experiences no volume change. The strain mismatch, which results in mechanical instability and hence the poor cycle stability, was reduced by reducing A/I interface area, which was realized by reducing diameter of Cu bonded Ni–Sn nanowires.

To optimize the performance of the Ni–Sn nanowire electrodes, the effect of the nanowire composition on the electrochemical performance of Li-ion batteries were studied. Ni–Sn nanowire arrays with 78 wt%, 82.1 wt%, and 86.7 wt% Sn were electrochemically deposited at voltages of −1.4 V, −1.2 V, and −1.0 V, respectively. Fig. 6(a) shows the effect of the nanowire composition on the electrochemical performance of Li-ion batteries using

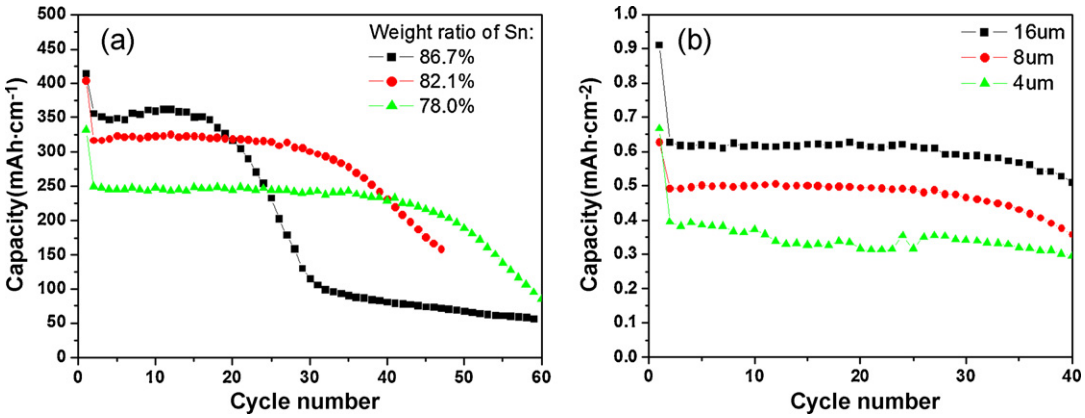

Fig. 6. (a) The effect of composition on the electrochemical performance of Cu nanorods-bonded Ni–Sn nanowires. The length of all nanowires is 8 μm. (b) The effect of the length of nanowires on the electrochemical performance of Cu-bonded Ni–Sn nanowire arrays with 82.1% Sn composition. For both (a) and (b), the diameter of the Ni–Sn nanowires is 200 nm, and the test current is 50 mA g^{-1}.

Cu nanoscrew-bonded Ni–Sn nanowires as anode. With increasing the percentage of Sn in the Ni–Sn alloys, specific capacity of the electrode increases but the stability decreases. This result is consistent with the theoretical prediction about Ni–Sn film electrodes where Ni acts as the inactive matrix to accommodate volume change [28].

Areal capacity, which is the capacity delivered per unit area on the plain surface of an electrode, is an important parameter to evaluate performance of electrodes [34]. High areal capacity of electrodes ensures high energy density of batteries by reducing the amount of accessory parts such as separators and mechanical support. High areal capacity can be easily realized with nanowire electrodes by growing long nanowires to increase the mass loading. Fig. 6(b) shows the effect of the nanowire length on the areal capacity of Cu-bonded Ni–Sn nanowire anode. The longer the Ni–Sn nanowires are, the higher the areal capacity is. In addition, the samples with both 8 μm and 16 μm long Ni–Sn nanowires show much higher areal capacity than reported results of Ni–Sn thin films, which are around 0.3–0.4 mAh cm^{-2} [29]. The capacity of the 16 μm long nanowire sample is 0.64 mAh cm^{-2} at stable stage while that of the 8 μm long nanowire sample is 0.5 mAh cm^{-2}.

Finally, we have improved capacity and cycling stability of the Ni–Sn nanowire electrodes by reducing the effect of strain mismatch at active/inactive interfaces in this study. However, due to the large volume change of the Ni–Sn alloys during cycling [29,35], their cycling stability is still not satisfying, especially when the percentage of Sn in the Ni–Sn alloys was increased. The performance of Ni–Sn nanowire electrodes can be improved with further treatments, such as Al_2O_3 coating for protection and buffer layer for strain-graded structure [36,37].

4. Conclusions

A porous anodic alumina (PAA) template-assisted electrochemical deposition method was used to directly synthesize Ni–Sn nanowire arrays on Cu current collectors. Formation of a continuous Ni–Sn film at the base introduces a large continuous (A/I) interface, which leads to the weak mechanical stability due to large strain mismatch. By growing short Cu nanoscrews as a buffer layer before Ni–Sn nanowire growth, the A/I interface was scaled down to nanoscale islands, which resulted in enhanced structural stability and battery performance. Further reduction of A/I interface by reducing the nanowire diameter of Cu-bonded nanowires results in even more stable electrode.

Acknowledgments

This work is supported by a University of Colorado Innovative Seed Grant and the Defense Advanced Research Projects Agency (DARPA) N/MEMS S&T Fundamentals program through the DARPA Center on Nanoscale Science and Technology for Integrated Micro/Nano-Electromechanical Transducers (iMINT) under grant no. N66001-10-1-4007 issued by the Space and Naval Warfare Systems Center Pacific (SPAWAR). This research was supported in part by the NNIN at the Colorado Nanofabrication Laboratory and the National Science Foundation under Grant No. ECS-0335765.

References

[1] S. Megahed, W. Ebner, J. Power Sources 54 (1995) 155–162.
[2] S. Prakash, W.E. Mustain, P.A. Kohl, J. Power Sources 189 (2009) 1184–1189.
[3] E. Karden, S. Ploumen, B. Fricke, T. Miller, K. Snyder, J. Power Sources 168 (2007) 2–11.
[4] P.G. Bruce, B. Scrosati, J.M. Tarascon, Angew. Chem. Int. Ed. 47 (2008) 2930–2946.
[5] N.C. Li, C.R. Martin, B. Scrosati, J. Power Sources 97–98 (2001) 240–243.
[6] C.R. Sides, N.C. Li, C.J. Patrissi, B. Scrosati, C.R. Martin, MRS Bull. 27 (2002) 604–607.
[7] H. Zhang, X. Yu, P. Braun, Nat. Nanotechnol. 6 (2011) 277–281.
[8] A.R. Armstrong, G. Armstrong, J. Canales, P.G. Bruce, J. Power Sources 146 (2005) 501–506.
[9] Y.G. Li, B. Tan, Y.Y. Wu, J. Am. Chem. Soc. 128 (2006) 14258–14259.
[10] C.K. Chan, X.F. Zhang, Y. Cui, Nano Lett. 8 (2008) 307–309.
[11] Y. Cui, Nat. Nanotechnol. 3 (2008) 31.
[12] Y.G. Li, B. Tan, Y.Y. Wu, Nano Lett. 8 (2008) 265–270.
[13] A.R. Armstrong, G. Armstrong, J. Canales, R. Garcia, P.G. Bruce, Adv. Mater. (Weinheim, Germany) 17 (2005) 862–865.
[14] P.L. Tabernal, S. Mitra, Nat. Mater. 5 (2006) 567.
[15] M.S. Park, G.X. Wang, Y.M. Kang, D. Wexler, S.X. Dou, H.K. Liu, Angew. Chem. Int. Ed. 46 (2007) 750–753.
[16] K.T. Nam, D.W. Kim, P.J. Yoo, C.Y. Chiang, N. Meethong, P.T. Hammond, Y.M. Chiang, A.M. Belcher, Science 312 (2006) 885–888.
[17] C.K. Chan, H.L. Peng, R.D. Twesten, K. Jarausch, X.F. Zhang, Y. Cui, Nano Lett. 7 (2007) 490–495.
[18] J.P. Maranchi, A.F. Hepp, A.G. Evans, N.T. Nuhfer, P.N. Kumta, J. Electrochem. Soc. 153 (2006) A1246–A1253.
[19] L.Y. Beaulieu, K.W. Eberman, R.L. Turner, L.J. Krause, J.R. Dahn, Electrochem. Solid State Lett. 4 (2001) A137–A140.
[20] B.M. Kim, G.B. Cho, J.P. Noh, H.J. Ahn, E.S. Choi, S. Miyazaki, T.H. Nam, J. Alloys Compd. 497 (2010) L13–L16.
[21] T. Zhang, H.P. Zhang, L.C. Yang, B. Wang, Y.P. Wu, T. Takamur, Electrochim. Acta 53 (2008) 5660–5664.
[22] M. Uehara, J. Suzuki, K. Tamura, K. Sekine, T. Takamura, J. Power Sources 146 (2005) 441–444.
[23] W. Wang, P.N. Kumta, ACS Nano 4 (2010) 2233–2241.
[24] S.A. Sapp, B.B. Lakshmi, C.R. Martin, Adv. Mater. (Weinheim, Germany) 11 (1999) 402–404.
[25] G. Sauer, G. Brehm, S. Schneider, K. Nielsch, R.B. Wehrspohn, J. Choi, H. Hofmeister, U. Gosele, J. Appl. Phys. 91 (2002) 3243.
[26] J. Hassoun, S. Panero, P. Simon, P.L. Taberna, B. Scrosati, Adv. Mater. 19 (2007) 1632.

[27] A. Bund, D. Thiemig, J. Appl. Electrochem. 37 (2007) 345–351.
[28] H. Mukaibo, T. Sumi, T. Yokoshima, T. Momma, T. Osaka, Electrochem. Solid State Lett. 6 (2003) A218–A220.
[29] J. Hassoun, S. Panero, B. Scrosati, J. Power Sources 160 (2006) 1336–1341.
[30] J.J. Zhang, Y.Y. Xia, J. Electrochem. Soc. 153 (2006) A1466–A1471.
[31] H. Mukaibo, T. Momma, M. Mohamedi, T. Osaka, J. Electrochem. Soc. 152 (2005) A560–A565.
[32] U. Kasavajjula, C. Wang, A. Appleby, J. Power Sources 163 (2007) 1003–1039.
[33] R. Deshpande, Y.T. Cheng, M.W. Verbrugge, J. Power Sources 195 (2010) 5081–5088.
[34] G.M. Ehrlich, C. Durand, X. Chen, T.A. Hugener, F. Spiess, S.L. Suib, J. Electrochem. Soc. 147 (2000) 886–891.
[35] I. Amadei, S. Panero, B. Scrosati, G. Cocco, L. Schiffini, J. Power Sources 143 (2005) 227–230.
[36] S.T. Myung, K. Izumi, S. Komaba, Y.K. Sun, H. Yashiro, N. Kumagai, Chem. Mater. 17 (2005) 3695–3704.
[37] N. Koratkar, R. Krishnan, T.M. Lu, Nano Lett. 11 (2011) 377–384.